Pulsed quantum optomechanics

M. R. Vanner[a,1], I. Pikovski[a], G. D. Cole[a], M. S. Kim[b], Č. Brukner[a,c], K. Hammerer[c,d], G. J. Milburn[e], and M. Aspelmeyer[a]

[a]Vienna Center for Quantum Science and Technology (VCQ), Faculty of Physics, University of Vienna, Boltzmanngasse 5, A-1090 Vienna, Austria; [b]QOLS (Quantum Optics and Laser Science Group), Blackett Laboratory, Imperial College London, London SW7 2BW, United Kingdom; [c]Institute for Quantum Optics and Quantum Information (IQOQI) of the Austrian Academy of Sciences, A-1090 Vienna and A-6020 Innsbruck, Austria; [d]Institute for Theoretical Physics and Albert Einstein Institute, University of Hannover, Callinstrasse 38, D-30167 Hannover, Germany; and [e]School of Mathematics and Physics, University of Queensland, Saint Lucia 4072, Australia

Edited by Mikhail Lukin, Harvard University, Cambridge, MA, and accepted by the Editorial Board July 21, 2011 (received for review April 1, 2011)

Studying mechanical resonators via radiation pressure offers a rich avenue for the exploration of quantum mechanical behavior in a macroscopic regime. However, quantum state preparation and especially quantum state reconstruction of mechanical oscillators remains a significant challenge. Here we propose a scheme to realize quantum state tomography, squeezing, and state purification of a mechanical resonator using short optical pulses. The scheme presented allows observation of mechanical quantum features despite preparation from a thermal state and is shown to be experimentally feasible using optical microcavities. Our framework thus provides a promising means to explore the quantum nature of massive mechanical oscillators and can be applied to other systems such as trapped ions.

optomechanics | quantum measurement | squeezed states

Coherent quantum mechanical phenomena, such as entanglement and superposition, are not apparent in the macroscopic realm. It is currently held that on large scales quantum mechanical behavior is masked by decoherence (1) or that quantum mechanical laws may even require modification (2–5). Despite substantial experimental advances, see for example ref. 6, probing this regime remains extremely challenging. Recently however, it has been proposed to utilize the precision and control of quantum optical fields in order to investigate the quantum nature of massive mechanical resonators by means of the radiation-pressure interaction (7–13). Quantum state preparation and the ability to probe the dynamics of mechanical oscillators, the most rigorous method being quantum state tomography, are essential for such investigations. These important elements have been experimentally realized for various quantum systems, e.g., light (14, 15), trapped ions (16, 17), atomic ensemble spin (18, 19), and intracavity microwave fields (20). By contrast, an experiment realizing both quantum state preparation and tomography of a mechanical resonator is yet to be achieved. Also, schemes that can probe quantum features without full tomography [e.g., (9, 10, 21)] are similarly challenging. In nanoelectromechanics, cooling of resonator motion and preparation of the ground state have been observed (22, 23) but quantum state reconstruction (24) remains outstanding. In cavity optomechanics significant experimental progress has been made towards quantum state control over mechanical resonators (11–13), which includes classical phase-space monitoring (25, 26), laser cooling close to the ground state (27, 28), and low noise continuous measurement of mechanically induced phase fluctuations (29–31). Still, quantum state preparation is technically difficult primarily due to thermal bath coupling and weak radiation-pressure interaction strength, and quantum state reconstruction remains little explored. Thus far, a common theme in proposals for mechanical state reconstruction is state transfer to and then read-out of an auxillary quantum system (32–35). This technique is a technically demanding approach and remains a challenge.

In this paper we introduce an optomechanical scheme that provides direct access to all the mechanical quadratures in order to obtain full knowledge about the quantum state of mechanical motion. This quadrature access is achieved by observing the distribution of phase noise of strong pulses of light at various times throughout a mechanical period. We show that the same experimental tools used for quantum state tomography can also be used for squeezed state preparation and state purification, which thus provides a complete experimental framework. Our scheme does not require "cooling via damping" (11–13) and can be performed within a single mechanical cycle thus significantly relaxing the technical requirements to minimize thermal contributions from the environment.

Using a pulsed interaction that is very short compared to the period of an oscillator to provide a back-action-evading measurement of position was introduced in the seminal contributions of Braginsky and coworkers (36, 37), where schemes for sensitive force detection were developed. In our work, the quantum nature of a mechanical resonator is itself the central object of investigation. Here, the pulsed interaction is used to provide an experimentally feasible means to generate and fully reconstruct quantum states of mechanical motion. The proposed experimental setup is shown in Fig. 1. A pulse of duration much less than the mechanical period is incident upon an optomechanical Fabry-Pérot cavity which we model as being single sided. Due to the entanglement generated during the radiation-pressure interaction, the optical phase becomes correlated with the mechanical position while the optical intensity imparts momentum to the mechanical oscillator. Time-domain homodyne detection (15) is then used to determine the phase of the field emerging from the cavity, and thus to obtain a measurement of the mechanical position. For each pulse, the measurement outcome P_L is recorded, which for Gaussian optical states has mean and variance

$$\langle P_L \rangle = \chi \langle X_M^{\text{in}} \rangle, \qquad \sigma_{P_L}^2 = \sigma_{P_L^{\text{in}}}^2 + \chi^2 \sigma_{X_M^{\text{in}}}^2, \qquad [1]$$

respectively. X_M^{in} is the mechanical position quadrature immediately prior to the interaction and P_L^{in} describes the input phase of light. The position measurement strength χ is an important parameter in this work as it quantifies the scaling of the mechanical position information onto the light field. A derivation of Eq. **1** including an optimization of χ by determining the input pulse envelope to gain the largest cavity enhancement is provided in the *Appendix*.

In order to describe and quantify the pulse interaction and measurement we use the nonunitary operator Υ that determines the new mechanical state via $\rho_M^{\text{out}} \propto \Upsilon \rho_M^{\text{in}} \Upsilon^\dagger$. This operator is mechanical state independent and can be determined from the probability density of measurement outcomes

$$\Pr(P_L) = \text{Tr}_M(\Upsilon^\dagger \Upsilon \rho_M^{\text{in}}). \qquad [2]$$

For pure optical input, it takes the form

Author contributions: M.R.V., I.P., G.D.C., M.S.K., Č.B., K.H., G.J.M., and M.A. designed research; M.R.V., I.P., G.D.C., M.S.K., Č.B., K.H., G.J.M., and M.A. performed research; and M.R.V., I.P., G.D.C., M.S.K., Č.B., K.H., G.J.M., and M.A. wrote the paper.

The authors declare no conflict of interest.

This article is a PNAS Direct Submission. M.L. is a guest editor invited by the Editorial Board.

Freely available online through the PNAS open access option.

[1]To whom correspondence should be addressed. E-mail: michael.vanner@univie.ac.at.

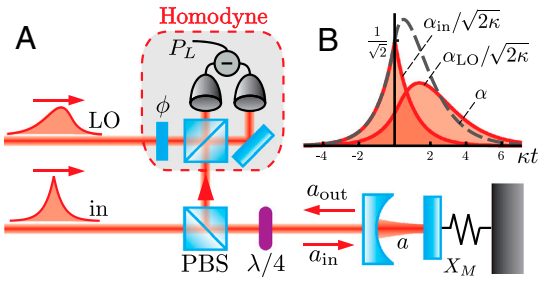

Fig. 1. (*A*) Schematic of the optical setup to achieve measurement based quantum state engineering and quantum state tomography of a mechanical resonator. An incident pulse (in) resonantly drives an optomechanical cavity, where the intracavity field *a* accumulates phase with the position quadrature X_M of a mechanical oscillator. The field emerges from the cavity (out) and balanced homodyne detection is used to measure the optical phase with a local oscillator pulse (LO) shaped to maximize the measurement of the mechanical position. (*B*) Scaled envelopes of the optimal input pulse, its corresponding intracavity field and the optimal local oscillator as computed in the *Appendix*.

$$\Upsilon = (\pi 2\sigma^2_{P_L^{\rm in}})^{-\frac{1}{4}} \exp\left[i\Omega X_M - \frac{(P_L - \chi X_M)^2}{4\sigma^2_{P_L^{\rm in}}}\right], \qquad [3]$$

where Ω quantifies the momentum transfer to the mechanics due to the pulse mean photon number. Υ can be readily understood by considering its action on a mechanical position wavefunction. This operator selectively narrows the wavefunction to a width scaling with χ^{-2} about a position which depends upon the measurement outcome. Moreover, the quantum non-demolition-like nature of Υ allows for back-action-evading measurements of X_M, i.e., the back-action noise imparted by the quantum measurement process occurs in the momentum quadrature only*. Other methods, such as the continuous variational measurement scheme (38), which has recently been considered for gravitational-wave detectors (39, 40), also allow for back-action-evading measurements. However, using short pulses offers a technically simpler route for quantum state tomography and is readily implementable, as will be discussed below.

In the following, we consider coherent drive i.e., $\sigma^2_{P_L^{\rm in}} = 1/2$. We first address the important challenge of how to experimentally determine the motional quantum state of a mechanical resonator. We then discuss how such a measurement can be used for quantum state preparation and finally we provide details for a physical implementation and analyze a thorough list of potential experimental limitations.

Mechanical Quantum State Tomography

Of vital importance to any experiment aiming to explore quantum mechanical phenomena is a means to measure coherences and complementary properties of the quantum system. Such measurement is best achieved by complete quantum state tomography, which despite being an important quantum optical tool has received very little attention for mechanical resonators†. Any measurement made on a single realization of a quantum state cannot yield sufficient information to characterize that quantum state. The essence of quantum state tomography is to make measurements of a specific set of observables over an ensemble of identically prepared realizations. The set is such that the measurement results provide sufficient information for the quantum state to be uniquely determined. One such method is to measure the marginals $\langle X|e^{-i\theta n}\rho e^{i\theta n}|X\rangle$, where n is the number operator, for all phase-space angles θ, see refs. 14, 15, 42 and e.g., ref. 43.

Our scheme provides a means for precision measurement of the mechanical quadrature marginals, thus allowing the mechanical quantum state to be determined. Specifically, given a mechanical state $\rho_M^{\rm in}$, harmonic evolution of angle $\theta = \omega_M t$ provides access to all the quadratures of this mechanical quantum state which can then be measured by a subsequent pulse. Thus, reconstruction of any mechanical quantum state can be performed. The optical phase distribution Eq. **2**, including this harmonic evolution, becomes

$$\Pr(P_L) = \int \frac{dX_M}{\sqrt{\pi}} e^{-(P_L - \chi X_M)^2} \langle X_M|e^{-i\theta n}\rho_M^{\rm in} e^{i\theta n}|X_M\rangle, \qquad [4]$$

which is a convolution between the mechanical marginal of interest and a kernel that is dependent upon χ and the quantum phase noise of light. The effect of the convolution is to broaden the marginals and to smooth any features present.

Let us consider the specific example of a mechanical resonator in a superposition of two coherent states, i.e., $|\psi_\delta\rangle \propto |i\delta\rangle + |-i\delta\rangle$. The X_M marginal of this mechanical Schrödinger-cat state contains oscillations on a scale smaller than the ground state. The convolution scales the amplitude of these oscillations by $\exp(-\frac{2\delta^2}{\chi^2+1})$ and thus for small χ they become difficult to resolve in the optical phase noise distribution. Shown in Fig. 2 are marginals of the mechanical state $|\psi_\delta\rangle$ and the optical phase distributions that would be observed according to Eq. **4**. Scaling the phase distribution by using the variable P_L/χ provides an approximation to the mechanical marginals, which becomes more accurate with increasing χ and may even show the interference features in a superposition state. Indeed, the limiting case of infinite χ corresponds to a von-Neumann projective measurement of the mechanical position, such that the distribution obtained for P_L/χ becomes identical to the mechanical marginals. However, *the mechanical marginals can be recovered even for small measurement strength* χ. This recovery is achieved as follows: First, by fixing the length of the cavity the optical phase distribution can be observed without contributions from mechanical position fluctuations. This rigidity allows measurement of the convolution kernel for a particular χ (determined by the proper-

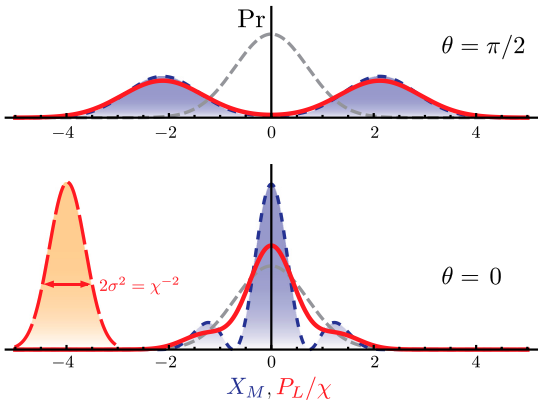

Fig. 2. The scheme presented here provides an experimentally feasible means to obtain direct access to the marginals of a quantum state of a mechanical resonator. Shown are complementary quadrature marginals of the mechanical coherent state superposition $|\psi_\delta\rangle \propto |i\delta\rangle + |-i\delta\rangle$, for $\delta = 1.5$ (blue dashed lines with fill, plotted with X_M). The mechanical ground state is shown for comparison in gray dashed lines. The two population components are seen for the quadrature angle $\theta = \pi/2$ and the quantum interference fringes for $\theta = 0$. A coherent optical pulse is used to probe the mechanical state where its phase quadrature becomes the convolution between the intrinsic phase noise, with variance scaling with χ^{-2}, and the mechanical marginal (red solid lines, plotted with P_L/χ where $\chi = 2$), see Eq. **4**. The convolution kernel can be observed by using a fixed length cavity, shown in the $\theta = 0$ plot (red dashed line with fill, fixed length with $X_M = -4$), which allows for accurate recovery of the mechanical marginals even for a weak measurement strength χ.

*No mechanical position noise is added as our measurement operator commutes with the mechanical position. This is because the mechanical evolution can be neglected during the short optomechanical interaction.

†During the submission process of this manuscript a scheme to perform tomography of the motional state of a trapped particle using a time-of-flight expansion was proposed (41).

ties of the mechanical resonator of interest, cavity geometry, and pulse strength, see Eq. **14**). With χ and the kernel known one can then perform deconvolution to determine the mechanical marginals. The performance of such a deconvolution is limited by experimental noise in the calibration of χ and the measurement of $\Pr(P_L)$. However, it is expected that these quantities can be accurately measured as quantum noise limited detection is readily achieved.

Mechanical Quantum State Engineering and Characterization

We now discuss how the measurement affects the mechanical state. First, we consider Υ acting on a mechanical coherent state $|\beta\rangle$. By casting the exponent of Υ in a normal ordered form, one can show that the resulting mechanical state, which is conditioned on measurement outcome P_L, is $\mathcal{N}_\beta \Upsilon|\beta\rangle = S(r)D(\mu_\beta)|0\rangle$. Here, $\mathcal{N}_\beta$ is a β-dependent normalization, D is the displacement operator for $\mu_\beta = (\sqrt{2}\beta + i\Omega + \chi P_L)/\sqrt{2(\chi^2+1)}$, and S is the squeezing operator, which yields the position width $2\sigma^2_{X_M} = e^{-2r} = (\chi^2+1)^{-1}$.

In most experimental situations, the initial mechanical state is in a thermal state $\rho_{\bar{n}} = \frac{1}{\pi\bar{n}}\int d^2\beta e^{-|\beta|^2/\bar{n}}|\beta\rangle\langle\beta|$, quantified by its average phonon occupation number $\bar{n}$. The marginals of the resulting state after the action of Υ are

$$\langle X_M|e^{-i\theta n}\Upsilon\rho_{\bar{n}}\Upsilon^\dagger e^{i\theta n}|X_M\rangle \propto \exp\left[-\frac{(X_M - \langle X_M^\theta\rangle)^2}{2\sigma_\theta^2}\right], \qquad [5]$$

where

$$\langle X_M^\theta\rangle = \frac{\chi P_L}{\chi^2 + \frac{1}{1+2\bar{n}}}\cos(\theta) - \Omega\sin(\theta),$$
$$\sigma_\theta^2 = \frac{1}{2}\frac{\cos^2(\theta)}{\chi^2 + \frac{1}{1+2\bar{n}}} + \frac{1}{2}(\chi^2 + 1 + 2\bar{n})\sin^2(\theta) \qquad [6]$$

are the mean and variance of the resulting conditional state, respectively. For large initial occupation (provided thermal fluctuations are negligible during the short interaction), the resultant position quadrature of the mechanics has mean $\langle X_M^{\theta=0}\rangle \simeq P_L/\chi$ and width $2\sigma^2_{\theta=0} \simeq \chi^{-2}$. Thus, squeezing in the X_M quadrature below the ground state is obtained when $\chi > 1$ and is *independent of the initial thermal occupation of the mechanics.* We have thus shown how the remarkable behavior of quantum measurement (also used in refs. 18–20, 44–47) can be experimentally applied to a mechanical resonator for quantum state preparation.

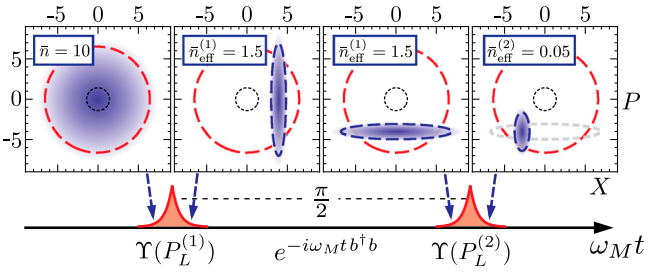

Fig. 3. Wigner functions of the mechanical state (above) at different times (indicated by arrows) during the experimental protocol (below). From left: Starting with an initial thermal state $\bar{n} = 10$, (this is chosen to ensure the figure dimensions are reasonable,) a pulsed measurement is made with $\chi = 1.5$ and outcome $P_L^{(1)} = 4\chi$ obtained, which yields an X_M quadrature squeezed state. The mechanical state evolves into a P_M quadrature squeezed state following free harmonic evolution of 1/4 of a mechanical period prior to a second pulse with outcome $P_L^{(2)} = -3\chi$ yielding the high-purity mechanical squeezed state. The effective thermal occupation of the mechanical states during the protocol is indicated. The final state's occupation can be reduced below unity even for large initial occupation, see Eq. **7** of the main text. Dashed lines indicate the 2σ-widths and the dotted lines show the ground state ($\bar{n} = 0$) for comparative purposes. The displacement Ω is not shown.

There is currently significant interest in the preparation of low entropy states of mechanical resonators as a starting point for quantum experiments, e.g., refs. 22, 23, 27, 28. The two main methods being pursued in optomechanics (11–13) are "passive cooling" which requires the stable operation of a (usually cryogenically compatible) high-finesse cavity, and "active cooling" which requires precision measurement and feedback. Closer in spirit to the latter, our pulsed measurement scheme provides a third method to realize high-purity states of the mechanical resonator. We quantify the state purity after measurement via an effective mechanical thermal occupation $\bar{n}_{\rm eff}$, which we define through $1 + 2\bar{n}_{\rm eff} = \sqrt{4\sigma^2_{\theta=0}\sigma^2_{\theta=\pi/2}}$. When acting on an initial thermal state, the measurement dramatically reduces uncertainty in the X_M quadrature, but leaves the thermal noise in the P_M quadrature unchanged: use of Eq. **6** for $\bar{n} \gg 1$ yields $\bar{n}^{(1)}_{\rm eff} \simeq \sqrt{\bar{n}/2\chi^2}$. The purity can be further improved by a second pulse, which is maximized for pulse separation $\theta = \omega_M t = \pi/2$, where the initial uncertainty in the momentum becomes the uncertainty in position. Such a sequence of pulses[‡] is represented in Fig. 3, where the resulting state was obtained akin to Eq. **5**. The effective occupation of the final state after two pulses is

$$\bar{n}^{(2)}_{\rm eff} \simeq \frac{1}{2}\left(\sqrt{1 + \frac{1}{\chi^4}} - 1\right), \qquad [7]$$

which is also independent of initial occupation. For $\chi > 1$, $\bar{n}^{(2)}_{\rm eff}$ is well below unity and therefore this scheme can be used as an alternative to "cooling via damping" for mechanical state purification.

Following state preparation, one can use a subsequent "read-out" pulse after an angle of mechanical free evolution θ to perform tomography. During state preparation however, the random measurement outcomes will result in random mechanical means Eq. **6**. This randomness can be overcome by recording and utilizing the measurement outcomes. One can achieve unconditional state preparation with use of appropriate displacement prior to the read-out pulse. Or, use postselection to analyze states prepared within a certain window. Alternatively, one may compensate during data analysis by appropriately adjusting each measurement outcome obtained during read-out. We now look at the latter option and consider a Gaussian mechanical state prepared by a prior pulsed measurement. The position distribution has variance σ^2 to be characterized and has a known mean $\langle X_M^{(p)}\rangle$, which is dependent upon the random measurement outcome. The read-out pulse will then have the distribution $\Pr(P_L) \propto \exp[(-(P_L - \chi\langle X_M^{(p)}\rangle)^2)/(1 + \chi^2 2\sigma^2)]$. For each read-out pulse, by taking $P_L|_p = P_L - \chi\langle X_M^{(p)}\rangle$ one can obtain the conditional variance $\sigma^2_{P_L|_p}$ for all θ to characterize the noise of the prepared Gaussian state. We note that this concept of compensating for a random but known mean can also be used to characterize non-Gaussian states.

Experimental Feasibility

We now provide a route for experimental implementation, discussing potential limitations and an experimentally feasible parameter regime. To ensure that the interaction time be much less than mechanical time scales the cavity decay rate κ must be much larger than the mechanical frequency. To this end, we consider the use of optical microcavities operating at $\lambda = 1{,}064$ nm, length 4λ and finesse of 7,000, which have an amplitude decay rate $\kappa/2\pi \simeq 2.5$ GHz. Such short cavity devices incorporating a micro-

[‡]We note that strong squeezing of an oscillator can also be achieved by using rapid modifications to the potential at quarter period intervals (48). However, we would like to emphasize that the squeezing we are discussing here does not arise from a parametric process, see e.g., ref. 49, rather it is due to the nonunitary action of measurement.

mechanical element as one of the cavity mirrors have previously been fabricated for tunable optical filters, vertical-cavity surface-emitting lasers and amplifiers (see for example ref. 50), but are yet to be considered for quantum optomechanical applications. Typically, these devices employ plane-parallel geometries, which places a severe constraint on the minimum lateral dimensions of the suspended mirror structure in order to minimize diffraction losses (51). Geometries using curved mirrors are required to reduce diffraction losses for the practical realization of high-finesse cavities. Presently, all realizations use a curved suspended mirror, see e.g., refs. 52, 53. However, in order to allow for enhanced freedom in the construction of the mechanical resonator, particularly with respect to the development of ultra-low loss mechanical devices (54), a flat suspended mirror is desired. In Fig. 4 our proposed fabrication procedure for such a device is shown. The small-mode-volume cavity considered here provides the bandwidth necessary to accommodate the short optical pulses and additionally offers a large optomechanical coupling rate. One technical challenge associated with these microcavities is fabrication with sufficient tolerance to achieve the desired optical resonance (under the assumption of a limited range of working wavelength), however this can be overcome by incorporating electrically controlled tunability of the cavity length (50, 52, 53).

For a mechanical resonator with eigenfrequency $\omega_M/2\pi =$ 500 kHz and effective mass $m = 10$ ng, the mechanical ground-state size is $x_0 = \sqrt{\hbar/m\omega_M} \simeq 1.8$ fm and optomechanical coupling proceeds at $g_0/2\pi = \omega_c(x_0/\sqrt{2}L)/2\pi \simeq 86$ kHz, where ω_c is the mean cavity frequency and L is the mean cavity length. The primary limitation in measurement strength is the optical intensity that can be homodyned before photodetection begins to saturate. Using pulses of mean photon number $N_p = 10^8$, which can be homodyned, yields $\Omega \simeq 10^4$ for the mean momentum transfer[§] and $\chi \simeq 1.5$. For this χ, the action of a single pulse on a large thermal state reduces the mechanical variance to $\sigma^2_{X_M} \simeq 0.2$, i.e., less than half the width of the ground state. With a second pulse after mechanical evolution the effective occupation [7] is $\bar{n}^{(2)}_{\text{eff}} \simeq 0.05$.

In order to observe mechanical squeezing, i.e., $\sigma^2_{X_M} < 1/2$, the conditional variance must satisfy $\sigma^2_{P_L|_p} < \sigma^2_{P_L^{\text{in}}} + \chi^2/2$, where additional noise sources that do not affect the mechanical state, e.g., detector noise, can be subsumed into $\sigma^2_{P_L^{\text{in}}}$. It is therefore necessary to have an accurate experimental calibration of χ to quantify the mechanical width. (Similarly, Ω must also be accurately known to determine the conditional mean, see Eq. **6**). This calibration can be performed in the laboratory as follows: For a fixed length cavity and a given pulse intensity, the length of the cavity is adjusted by a known amount (by a calibrated piezo for example) and the proportionality between the homodyne measurement outcomes and the cavity length is determined. The pulses are then applied to a mechanical resonator and χ is determined with knowledge of x_0 of the resonator. With χ known Ω can then also be measured by observing the displacement of the mechanical state after one-quarter of a period.

Finally we discuss practical limitations. Firstly, finite mechanical evolution during the interaction decreases the back-action-evading nature of the measurement, which is described in the *Appendix*. Such evolution is not expected to be a severe limitation in the proposed implementation considered here as $\omega_M/\kappa \simeq 10^{-4}$. Secondly, the optical measurement efficiency η, affected by optical loss, inefficient detection, and mode mismatch, yields a reduced measurement strength $\chi \to \sqrt{\eta}\chi$. And thirdly, in many situations coupling to other mechanical vibrational modes is expected. This coupling contributes to the measurement outcomes and yields a spurious broadening of the tomographic results for the mode of interest. In practice however, one can minimize these contributions by engineering mechanical devices with high effective masses for the undesired modes and tailoring the intensity profile of the optical spot to have good overlap with a particular vibrational profile (55).

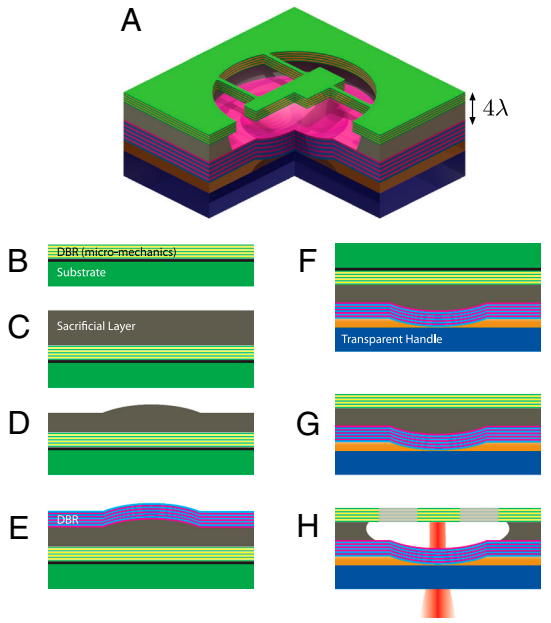

Fig. 4. Our proposed design and fabrication procedure for high-finesse optomechanical microcavities: Using microcavities provides optomechanical coupling rates many orders of magnitude larger than current millimeter or centimeter length scale implementations of optomechanical Fabry-Pérot cavities and can provide sufficient radiation-pressure interaction to resolve the small scale quantum properties of the mechanical resonator. (*A*) Cross-sectional view with a quarter of the device removed. Uppermost (colored green) is the mechanical resonator supported by auxiliary beams as was considered in ref. 54. The optical field is injected into the device from below through a transparent handle (colored blue) and the curved rigid input mirror (colored pink) and then resonates in the vacuum-gap between this and the mechanical device before being retroreflected. The design is a layered structure, fabricated in the following steps: (*B*) The base consists of a high-reflectivity distributed Bragg reflector (DBR) and an etch stop layer deposited on a suitable handle substrate. (*C*) First, a sacrificial film is deposited atop the DBR. (*D*) Next, a microlens pattern is transferred into the sacrificial layer through a reflow and reactive ion etching process. The radius of curvature of this structure is designed to match the phase front of the optical mode to minimize diffraction loss. (*E*) Following the microlens fabrication process a high reflectivity dielectric DBR is deposited over the sample surface. (*F*) The structure is then flipped and bonded to a transparent handle using a suitable low-absorption adhesive (e.g., spin on glass or UV-curable epoxy). (*G*) After mounting, the original growth substrate and etch stop are removed via chemo-mechanical etching. (*H*) Finally, the mechanical resonator is patterned and subsequently released via selective removal of the underlying sacrificial film. We remark that these integrated structures provide a platform for "on-chip" hybridization with other quantum systems.

Coupling to a Thermal Bath

For our tomography scheme the mechanical quantum state must not be significantly perturbed during the time scale ω_M^{-1}. To estimate the effect of the thermal bath following state preparation we consider weak and linear coupling to a Markovian bath of harmonic oscillators. For this model, assuming no initial correlations between the mechanics and the bath, the rethermalization scales with $\bar{n}\gamma_M$, where γ_M is the mechanical damping rate. It follows that an initially squeezed variance ($\chi > 1$) will increase to 1/2 on a time scale

$$\tau = \frac{Q}{\bar{n}\omega_M}\frac{1}{2}\left(1 - \frac{1}{\chi^2}\right). \qquad [8]$$

[§]This momentum is comparable to the width of a thermal state, i.e., $\Omega/\sqrt{\bar{n}} < 10$ for room temperature. Thus the mechanical motion remains harmonic.

Thus, for the parameters above and mechanical quality $Q = \omega_M/\gamma_M \simeq 10^5$ a temperature $T \lesssim 1$ K is required for the observation of squeezing during one mechanical period.

The state purification protocol, as shown in Fig. 3, is affected by rethermalization between the two pulsed measurements. This thermal process increases the effective thermal occupation and [7] is modified to

$$\bar{n}^{(2)}_{\rm eff}(T) \simeq \frac{1}{2}\left(\sqrt{1+\frac{1}{\chi^4}+\frac{\pi\bar{n}}{Q\chi^2}}-1\right). \quad [9]$$

For the above system parameters $\bar{n}^{(2)}_{\rm eff}(T = 1\ {\rm K}) \simeq 0.15$. Thus, mechanical state purification by measurement is readily attainable even at a modest bath temperature.

Moreover, we note that the position measurements of this scheme can be used to probe open system dynamics and thus provide an empirical means to explore decoherence and bath coupling models (56).

Conclusions

We have described a scheme to overcome the current challenge of quantum state reconstruction of a mechanical resonator, which provides a means to explore quantum mechanical phenomena on a macroscopic scale. Our experimental protocol allows for state purification, remote preparation of a mechanical squeezed state, and direct measurements of the mechanical marginals for quantum state reconstruction, thus providing a complete experimental framework. The experimental feasibility has been analyzed and we have shown that with the use of optomechanical microcavities this scheme can be readily implemented. The optomechanical entanglement generated by the pulsed interaction may also be a useful resource for quantum information processing. Moreover, the framework we have introduced can be built upon for further applications in quantum optomechanics and can be generalized to other systems, such as nanoelectromechanics and superconducting resonators, or used with dispersive interaction to study the motional state of mechanical membranes, trapped ions, or particles in a cavity.

Appendix

Model. The intracavity optomechanical Hamiltonian in the rotating frame at the cavity frequency is

$$H = \hbar\omega_M b^\dagger b - \hbar g_0 a^\dagger a(b+b^\dagger), \quad [10]$$

where a (b) is the optical (mechanical) field operator. The cavity field accumulates phase in proportion to the mechanical position and is driven by resonant radiation via the equation of motion

$$\frac{{\rm d}a}{{\rm d}t} = ig_0(b+b^\dagger)a - \kappa a + \sqrt{2\kappa}a_{\rm in}, \quad [11]$$

where κ is the cavity decay rate and $a_{\rm in}$ describes the optical input including drive and vacuum. During a pulsed interaction of time scale $\kappa^{-1} \ll \omega_M^{-1}$ the mechanical position is approximately constant. This constancy allows decoupling of Eq. **11** from the corresponding mechanical equation of motion and during the short interaction we have ${\rm d}b/{\rm d}t \simeq ig_0 a^\dagger a$, where we neglect the mechanical harmonic motion, mechanical damping, and noise processes. We write $a_{\rm in}(t) = \sqrt{N_p}\alpha_{\rm in}(t) + \tilde{a}_{\rm in}(t)$, where $\alpha_{\rm in}(t)$ is the slowly varying envelope of the drive amplitude with $\int {\rm d}t\alpha_{\rm in}^2 = 1$ and N_p is the mean photon number per pulse and similarly $a = \sqrt{N_p}\alpha(t) + \tilde{a}(t)$. Neglecting $ig_0(b+b^\dagger)\tilde{a}$ and approximating α as real, Eq. **11** becomes the pair of linear equations:

$$\frac{{\rm d}\alpha}{{\rm d}t} = \sqrt{2\kappa}\alpha_{\rm in} - \kappa\alpha, \quad [12]$$

$$\frac{{\rm d}\tilde{a}}{{\rm d}t} = ig_0\sqrt{N_p}(b+b^\dagger)\alpha + \sqrt{2\kappa}\tilde{a}_{\rm in} - \kappa\tilde{a}. \quad [13]$$

After solving for $\tilde{a}(t)$, the output field is then found by using the input-output relation $\tilde{a}_{\rm out} = \sqrt{2\kappa}\tilde{a} - \tilde{a}_{\rm in}$.

The mechanical position and momentum quadratures are $X_M = (b+b^\dagger)/\sqrt{2}$ and $P_M = i(b^\dagger - b)/\sqrt{2}$, respectively, the cavity (and its input/output) quadratures are similarly defined via $\tilde{a}$ ($\tilde{a}_{\rm in}/\tilde{a}_{\rm out}$). The statistics of the optical amplitude quadrature are unaffected by the interaction, however, the phase quadrature contains the phase dependent upon the mechanical position. The output phase quadrature emerging from the cavity is $P_L^{\rm out}(t) = \frac{g_0}{\kappa}\sqrt{N_p}\varphi(t)X_M^{\rm in} + 2\kappa e^{-\kappa t}\int_{-\infty}^{t}{\rm d}t' e^{\kappa t'}P_L^{\rm in}(t') - P_L^{\rm in}(t)$, where $\varphi(t) = (2\kappa)^{\frac{3}{2}}e^{-\kappa t}\int_{-\infty}^{t}{\rm d}t' e^{\kappa t'}\alpha(t')$ describes the accumulation of phase, $X_M^{\rm in}$ is the mechanical position prior to the interaction, and the last two terms are the input phase noise contributions. $P_L^{\rm out}$ is measured via homodyne detection, i.e., $P_L = \sqrt{2}\int {\rm d}t\alpha_{\rm LO}(t)P_L^{\rm out}(t)$. To maximize the measurement of the mechanical position the local oscillator envelope is chosen as $\alpha_{\rm LO}(t) = \mathcal{N}_\varphi\varphi(t)$, where $\mathcal{N}_\varphi$ ensures normalization. The contribution of $X_M^{\rm in}$ in P_L scales with $\chi = \sqrt{2}\frac{1}{\mathcal{N}_\varphi}\frac{g_0}{\kappa}\sqrt{N_p}$, which quantifies the mechanical position measurement strength. The mean and variance of P_L are given in Eq. **1** for pure Gaussian optical input and together with Ω and Eq. **2** are used to determine Υ, as given in Eq. **3**. We have thus arrived, for our physical setting, at an operator which is known from generalized linear measurement theory (see for example ref. 57). Also, we note that Eq. **3** is equivalent to $\Upsilon = e^{i\Omega X_M}\langle P_L|e^{i\chi X_L X_M}|0\rangle$, though the nonunitary process of cavity filling and decay is not explicit. We also remark that the construction of Υ can be readily generalized to include non-Gaussian operations.

The maximum χ is obtained for the input drive $\alpha_{\rm in}(t) = \sqrt{\kappa}e^{-\kappa|t|}$. This maximization can be seen by noting that $\mathcal{N}_\varphi^{-2} = \int {\rm d}t\varphi^2(t)$, which in Fourier space is $\mathcal{N}_\varphi^{-2} \propto \int {\rm d}\omega(\omega^2+\kappa^2)^{-2}|\alpha_{\rm in}(\omega)|^2$. Hence, for such cavity-based measurement schemes, the optimal drive has Lorentzian spectrum. This drive, $\alpha(t)$ obtained from Eq. **12** and the local oscillator are shown in Fig. 1*B*. The resulting optimal measurement strength is given by

$$\chi = 2\sqrt{5}\frac{g_0}{\kappa}\sqrt{N_p}, \quad [14]$$

and the mean momentum transfer due to α^2 is $\Omega = \frac{3}{\sqrt{2}}\frac{g_0}{\kappa}N_p$.

We note that this optimization of the driving field may also be applied to cavity-enhanced pulsed measurement of the spin of an atomic ensemble (18, 19, 58) or the coordinate of a trapped ion/particle (59–61). Particularly in the latter case, this approach will broaden the repertoire of measurement techniques available and may lead to some interesting applications.

Finite Mechanical Evolution During Interaction. In the model used above we have assumed that the mechanical position remains constant during the pulsed optomechanical interaction. Including finite mechanical evolution, the intracavity field dynamics Eq. **13** must be determined simultaneously with the mechanical dynamics. In the mechanical rotating frame with the conjugate quadratures $\overline{X}_M, \overline{P}_M$ these dynamics are solved to first order in ω_M/κ resulting in the input-output relations:

$$\overline{P}_M^{\rm out} = \overline{P}_M^{\rm in} + \Omega + \mathcal{N}_1\chi X_{C1},$$

$$\overline{X}_M^{\rm out} = \overline{X}_M^{\rm in} - \frac{\omega_M}{\kappa}\xi_1\Omega - \frac{\omega_M}{\kappa}\chi\mathcal{N}_2 X_{C2},$$

$$P_L = P_L^{\rm in} + \chi(\overline{X}_M^{\rm in} + \frac{\omega_M}{\kappa}\xi_2\overline{P}_M^{\rm in}) + \chi\frac{\omega_M}{\kappa}\xi_3\Omega + \chi^2\frac{\omega_M}{\kappa}\mathcal{N}_3 X_{C3}, \quad [15]$$

where P_L still represents the measurement outcome, $\mathcal{N}_{1,2,3}$ and $\xi_{1,2,3}$ are input drive-dependent dimensionless parameters of order unity, the former normalizing the nonorthogonal amplitude quadrature temporal modes $X_{C1,2,3}$. The main effects of the finite mechanical evolution can be seen in P_L. (*i*) The mechanical quadrature measured has been rotated, which in terms of the nonrotating quadratures is $\overline{X}_M \simeq X_M + \frac{\omega_M}{\kappa}\xi_2 P_M$. Such a rotation poses no principle limitation to our scheme however this must be taken

into account for the measurement of a particular mechanical quadrature. (*ii*) Each pulsed measurement now has a nonzero mean proportional to Ω. This mean can be experimentally characterized and appropriately subtracted from the outcomes. (*iii*) P_L now includes a term proportional to the optical amplitude noise. This term decreases the back-action evading quality of the measurement and has arisen due to mechanical momentum noise gained from the optical amplitude quadrature evolving into position noise. The conditional variance of the rotated mechanical quadrature including these effects, for large initial occupation, is

$$\sigma^2_{\tilde{X}_M} \simeq \frac{1}{2}\left[\frac{1}{\chi^2} + \zeta^2\chi^2\left(\frac{\omega_M}{\kappa}\right)^2\right], \qquad [16]$$

where ζ is another drive-dependent parameter of order unity. The two competing terms here give rise to a minimum variance of $\zeta\omega_M/\kappa$ when $\chi^2 = \kappa/(\zeta\omega_M)$. Experimentally reasonable values of χ will lie much below this optimum point, however, as $\kappa \gg \omega_M$ for the parameters we consider, the broadening due to finite evolution is small and strong squeezing can be achieved.

ACKNOWLEDGMENTS. The kind hospitality provided by the University of Gdańsk (I.P.), the University of Queensland (M.R.V.) and the University of Vienna (G.J.M.) is acknowledged. We thank S. Hofer, N. Kiesel and M. Żukowski for useful discussion. We thank the Australian Research Council (ARC) (Grant FF0776191), United Kingdom Engineering and Physical Sciences Research Council (EPSRC) and the Royal Society, European Research Council (ERC) (StG QOM), European Commission (MINOS, Q-ESSENCE), Foundational Questions Institute (FQXi), Fonds zur Förderung der wissenschaftlichen Forschung (FWF) (L426, P19570, SFB FoQuS, START), Centre for Quantum Engineering and Space-Time Research (QUEST), and an ÖAD/MNiSW program for support. M.R.V. and I.P. are members of the FWF Doctoral Programme CoQuS (W 1210). M.R.V. is a recipient of a DOC fellowship of the Austrian Academy of Sciences. G.D.C. is a recipient of a Marie Curie Fellowship of the European Commission.

1. Zurek WH (2003) Decoherence, einselection, and the quantum origins of the classical. *Rev Mod Phys* 75:715–775.
2. Ghirardi GC, Rimini A, Weber T (1986) Unified dynamics for microscopic and macroscopic systems. *Phys Rev D* 34:470–491.
3. Diosi L (1989) Models for universal reduction of macroscopic quantum fluctuations. *Phys Rev A* 40:1165–1174.
4. Pearle P (1989) Combining stochastic dynamical state-vector reduction with spontaneous localization. *Phys Rev A* 39:2277–2289.
5. Penrose R (1996) On gravity's role in quantum state reduction. *Gen Relat Gravit* 28:581–600.
6. Hackermüller L, Hornberger K, Brezger B, Zeilinger A, Arndt M (2004) Decoherence of matter waves by thermal emission of radiation. *Nature (London)* 427:711–714.
7. Bose S, Jacobs K, Knight PL (1997) Preparation of nonclassical states in cavities with a moving mirror. *Phys Rev A* 56:4175–4186.
8. Bose S, Jacobs K, Knight PL (1999) Scheme to probe the decoherence of a macroscopic object. *Phys Rev A* 59:3204–3210.
9. Marshall W, Simon C, Penrose R, Bouwmeester D (2003) Towards quantum superpositions of a mirror. *Phys Rev Lett* 91:130401.
10. Kleckner D, et al. (2008) Creating and verifying a quantum superposition in a micro-optomechanical system. *New J Phys* 10:095020.
11. Kippenberg TJ, Vahala KJ (2008) Cavity optomechanics: back-action at the mesoscale. *Science* 321:1172–1176.
12. Marquardt F, Girvin S (2009) Optomechanics. *Physics* 2:40.
13. Aspelmeyer M, Groeblacher S, Hammerer K, Kiesel N (2010) Quantum optomechanics throwing a glance. *J Opt Soc Am B* 27:A189.
14. Smithey DT, Beck M, Raymer MG, Faridani A (1993) Measurement of the Wigner distribution and the density matrix of a light mode using optical homodyne tomography: application to squeezed states and the vacuum. *Phys Rev Lett* 70:1244–1247.
15. Lvovsky AI, Raymer MG (2009) Continuous-variable optical quantum-state tomography. *Rev Mod Phys* 81:299–332.
16. Leibfried D, et al. (1996) Experimental determination of the motional quantum state of a trapped atom. *Phys Rev Lett* 77:4281–4285.
17. Leibfried D, Blatt R, Monroe C, Wineland D (2003) Quantum dynamics of single trapped ions. *Rev Mod Phys* 75:281–324.
18. Kuzmich A, Mandel L, Bigelow NP (2000) Generation of spin squeezing via continuous quantum nondemolition measurement. *Phys Rev Lett* 85:1594–1597.
19. Appel J, et al. (2009) Mesoscopic atomic entanglement for precision measurements beyond the standard quantum limit. *Proc Natl Acad Sci USA* 106:10960–10965.
20. Deléglise S, et al. (2008) Reconstruction of non-classical cavity field states with snapshots of their decoherence. *Nature (London)* 455:510–514.
21. Armour A, Blencowe M, Schwab K (2002) Entanglement and decoherence of a micromechanical resonator via coupling to a cooper-pair box. *Phys Rev Lett* 88:148301.
22. Rocheleau T, et al. (2010) Preparation and detection of a mechanical resonator near the ground state of motion. *Nature (London)* 463:72–75.
23. O'Connell AD, et al. (2010) Quantum ground state and single-phonon control of a mechanical resonator. *Nature (London)* 464:697–703.
24. Rabl P, Shnirman A, Zoller P (2004) Generation of squeezed states of nanomechanical resonators by reservoir engineering. *Phys Rev B* 70:205304.
25. Tittonen I, et al. (1999) Interferometric measurements of the position of a macroscopic body: towards observation of quantum limits. *Phys Rev A* 59:1038–1044.
26. Briant T, Cohadon PF, Pinard M, Heidmann A (2003) Optical phase-space reconstruction of mirror motion at the attometer level. *Eur Phys J D* 22:131–140.
27. Groeblacher S, et al. (2009) Demonstration of an ultracold micro-optomechanical oscillator in a cryogenic cavity. *Nature Physics* 5:485–488.
28. Schliesser A, Arcizet O, Riviere R, Anetsberger G, Kippenberg TJ (2009) Resolved-sideband cooling and position measurement of a micromechanical oscillator close to the Heisenberg uncertainty limit. *Nature Physics* 5:509–514.
29. Teufel JD, Donner T, Castellanos-Beltran MA, Harlow JW, Lehnert KW (2009) Nanomechanical motion measured with an imprecision below that at the standard quantum limit. *Nat Nanotechnol* 4:820–823.
30. Anetsberger G, et al. (2010) Measuring nanomechanical motion with an imprecision below the standard quantum limit. *Phys Rev A* 82:061804(R).
31. Clerk AA, Girvin SM, Marquardt F, Schoelkopf RJ (2010) Introduction to quantum noise, measurement, and amplification. *Rev Mod Phys* 82:1155–1208.
32. Zhang J, Peng K, Braunstein S (2003) Quantum-state transfer from light to macroscopic oscillators. *Phys Rev A* 68:013808.
33. Woolley M, Doherty A, Milburn G, Schwab K (2008) Nanomechanical squeezing with detection via a microwave cavity. *Phys Rev A* 78:062303.
34. Singh S, Meystre P (2010) Atomic probe Wigner tomography of a nanomechanical system. *Phys Rev A* 81:041804(R).
35. Marek P, Filip R (2010) Noise-resilient quantum interface based on quantum nondemolition interactions. *Phys Rev A* 81:042325.
36. Braginsky VB, Vorontsov YI, Khalili FY (1978) Optimal quantum measurements in detectors of gravitation radiation. *JETP Lett+* 27:276–280.
37. Braginsky VB, Khalili FY (1992) *Quantum Measurement* (Cambridge University Press, United Kingdom).
38. Vyatchanin SP, Matsko AB (1993) Quantum limit on force measurements. *JETP Lett+* 77:218–221.
39. Mueller-Ebhardt H, et al. (2009) Quantum-state preparation and macroscopic entanglement in gravitational-wave detectors. *Phys Rev A* 80:043802.
40. Miao H, et al. (2010) Probing macroscopic quantum states with a sub-Heisenberg accuracy. *Phys Rev A* 81:012114.
41. Romero-Isart O, et al. (2011) Optically levitating dielectrics in the quantum regime: theory and protocols. *Phys Rev A* 83:013803.
42. Vogel K, Risken H (1989) Determination of quasiprobability distributions in terms of probability distributions for the rotated quadrature phase. *Phys Rev A* 40:2847–2849.
43. Dunn TJ, Walmsley IA, Mukamel S (1995) Experimental determination of the quantum-mechanical state of a molecular vibrational mode using fluorescence tomography. *Phys Rev Lett* 74:884–887.
44. Levenson MD, Shelby RM, Reid M, Walls DF (1986) Quantum nondemolition detection of optical quadrature amplitudes. *Phys Rev Lett* 57:24732476.
45. La Porta A, Slusher RE, Yurke B (1989) Back-action evading measurements of an optical field using parametric down conversion. *Phys Rev Lett* 62:28–31.
46. Roch J-F, et al. (1997) Quantum nondemolition measurements using cold trapped atoms. *Phys Rev Lett* 78:634–637.
47. Hammerer K, Aspelmeyer M, Polzik ES, Zoller P (2009) Establishing Einstein-Poldosky-Rosen channels between nanomechanics and atomic ensembles. *Phys Rev Lett* 102:020501.
48. Janszky J, Adam P (1992) Strong squeezing by repeated frequency jumps. *Phys Rev A* 46:6091–6092.
49. Walls DF (1983) Squeezed states of light. *Nature (London)* 306:141–146.
50. Cole GD, Behymer E, Bond TC, Goddard LL (2008) Short-wavelength MEMS-tunable VCSELs. *Opt Express* 16:16093–16103.
51. Riazi A (1981) Resonator equation relating Fresnel number, finesse, and number of beam transits. *Appl Optics* 20:3469–3470.
52. Tayebati P, et al. (1998) Half-symmetric cavity tunable microelectromechanical VCSEL with single spatial mode. *IEEE Photonic Tech L* 10:1679–1681.
53. Riemenschneider F, Aziz M, Halbritter H, Sagnes I, Meissner P (2002) Low-cost electrothermally tunable optical microcavities based on GaAs. *IEEE Photonic Tech L* 14:1566–1568.
54. Cole GD, Wilson-Rae I, Werbach K, Vanner MR, Aspelmeyer M (2010) Phonon-tunnelling dissipation in mechanical resonators. *Nature Communications* 2:231.
55. Pinard M, Hadjar Y, Heidmann A (1999) Effective mass in quantum effects of radiation pressure. *Eur Phys J D* 7:107–116.
56. Breuer H-P, Petruccione F (2002) *The Theory of Open Quantum Systems* (Oxford University Press, United Kingdom).
57. Caves CM, Milburn GJ (1987) Quantum-mechanical model for continuous position measurements. *Phys Rev A* 36:5543–5555.
58. Teper I, Vrijsen G, Lee J, Kasevich MA (2008) Backaction noise produced via cavity-aided nondemolition measurement of an atomic clock state. *Phys Rev A* 78:051803(R).
59. Jost JD, et al. (2009) Entangled mechanical oscillators. *Nature (London)* 459:683–685.
60. Chang DE, et al. (2010) Cavity opto-mechanics using an optically levitated nanosphere. *Proc Natl Acad Sci USA* 107:1005–1010.
61. Romero-Isart O, Juan ML, Quidant R, Cirac JI (2010) Toward quantum superposition of living organisms. *New J Phys* 12:033015.